Faculty of Applied Sciences
University of West Bohemia

Numerical study of joint of C/C composite fan to metal component using finite element method

Bachelor Thesis

Author: Anna Fictumová
Supervisor: Ing. Jan Bartošek

Submission Date: August, 2014

This is to certify that:

(i) the thesis comprises only my original work toward the Bachelor Degree

(ii) due acknowlegement has been made in the text to all other material used

(i) tímto prohlašuji, že jsem bakalářskou práci vypracovala samostatně

(ii) výlučně za použití citovaných pramenů

Anna Fictumová
August, 2014

Acknowledgments

I would like to express my sincere gratitude to my advisors Ing. Jan Bartošek, Dipl.-Ing. Gotthard Nauditt and Dr. Martin Henrich for always being there for me, no matter what. I would also like to say thank you to the Schunk Group for the bachelor thesis assignment.

Abstract

Research of metal-composite joints and C/C composite material was performed. Several design alternatives were modelled and their behaviour was numerically simulated. Strength and stiffness of individual designs were evaluated. Finally, an improvement of the shape of the critical part was suggested and numerically verified.

Abstrakt

V rámci bakalářské práce byla provedena rešerše spojů používaných pro spojení oceli a kompozotního materiálu C/C. Dále bylo numericky simulováno chování šroubového spoje. S ohledem na výsledky výpočtů, především hodnot pevnostního kritéria Tsai-Wu a velikosti síly působící na jednotlivé části spoje, bylo navrženo více alternativ provedení spoje, tyto byly namodelovány a jejich chování bylo posléze numericky simulováno. Na závěr byl navržen tvar části spoje lépe odpovídající působícímu zatížení. Jeho pevnost byla numericky ověřena.

Contents

Chapter 1

Introduction

"New times call for new ideas", an old proverb says. People are still trying to find solutions to the problems they face. This bachelor thesis is motivated by one of these problems, specifically an improvement of a metal fan. This fan was working well, but was unavailable in applications in high-temperature environments. That's why a new solution had to be found. The new fan was designed from carbon reinforced carbon composite (C/C) (Figure 1.1), which can handle high-temperature loading (up to 2800 °C), because it's stiffness and strength improve as the temperature rises. Even though a C/C fan has its advantages over a fan made from metal, its design is still limited by limited by many different constraints, e.g., the shape of the drive shaft and the material it is made from.

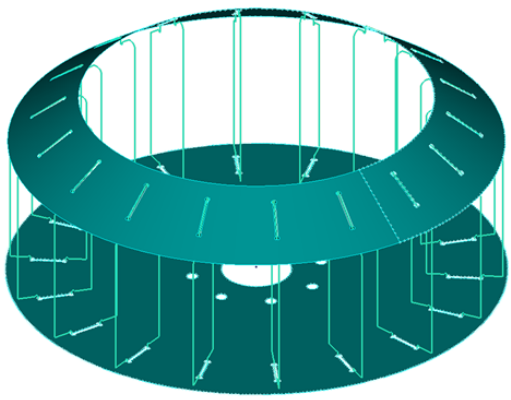

Figure 1.1: Model of C/C fan

Successful joining of two different materials, such as steel and C/C creates many design obstacles. Diverse thermal expansions cause diverse behaviour of fan parts which is followed by stress generation or conversely by pretension damage, depending on the joint type. For successful connection of two or more parts and especially for successful connection of parts made from different materials it is important to know the type of loading and to respect diverse behaviour of each material.

The goal of this thesis is to examine the loading which occurs in the C/C composite and the steel drive shaft joint. The first part of the thesis determines in which temperature the preload in the bolt joint disappears. The second part proposes and compares different solutions to the joint problem.

Chapter 2

Metal-Composite Joints

Mechanical joints allow to connect more materials or mechanical components together [11]. A plethora of different joint types exists. Each of them is designed for different applications, depending on the type of loading, materials and other required properties. Critical factors of the joint are, e.g, the load and load transfer types, whether the joint should be demountable or not, weight, size, jointed materials and environment. This chapter briefly describes the basic types of joints, which can be used to link composite materials and steel.

2.1 Bolted joints

Bolted joints are the most commonly used demountable joints and are advantageous thanks to their simplicity, reliability and possibility of dismantling without damaging any part of the assembly. The disadvantages include weight increase and lower stiffness when loaded by vibration.

Bolted joints are used for banding two parts of assembly together, if re-dismantling of the assembly is expected. Connection of two different parts of assembly with different properties is also appropriate. Bolted joints consist of a screw and a nut or a screw and a screw thread, which is drilled in one part of the assembly. The most important part of bolted joints is the screw thread. Bolted joint is shown in Figure 2.1.

Bolted joint is loaded by different types of loads shown in Figure 2.2. There, F_0 is the load, which ensures constriction of the nut. Due to this load, the thread is stretched and the sides of the joint are pressed. M_0 is the moment occurring due to inaccuracy of jointed surfaces. Other loads in the figure represent loading caused by use of the joint. During joint design, other problems than in "normal" steel-steel joint arise such as different directions of loading distribution in steel and composite. Sometimes, it is also important to use a corrosion barrier between the jointed parts such as glass/epoxy layer between graphite reinforced composites and aluminium screws [14].

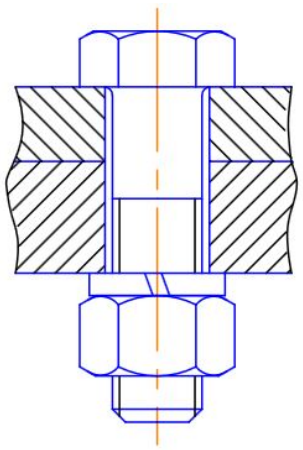

Figure 2.1: Bolted joint [1]

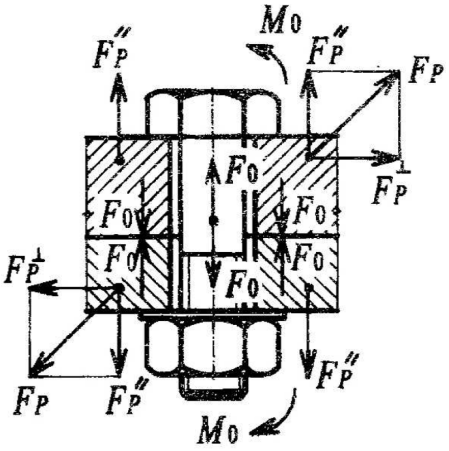

Figure 2.2: Loads and moments occuring in a bolted joint [10]

Figure 2.3: Fastening system linking a composite wheel and a metal wheel-seat [2]

Because composite materials are either orthotropic or anisotropic, danger of bearing failure or delamination ensues. To assure high bearing strength, laminate has to consist of plies with orientations 0, ±45 and 90 degrees. None of these orientations should be represented by more than 40 percent of all plies. To reduce the risk of delamination, laminate should include plies oriented under varied degrees [14]. Example of a bolted joint is shown in Figure 2.3.

2.2 Welded joints

A welded joint is one of the unmountable joints. Advantages of this type of coupling are stiffness, durability and low production costs. Welded joint merges two parts

of the assembly together and its properties are the same as properties of the linked parts. A bulge appears between the jointed parts and acts as a stress raiser. Therefore, it is necessary to monitor jointed area. An example of a welded joint between composite and steel is shown in Figure 2.4.

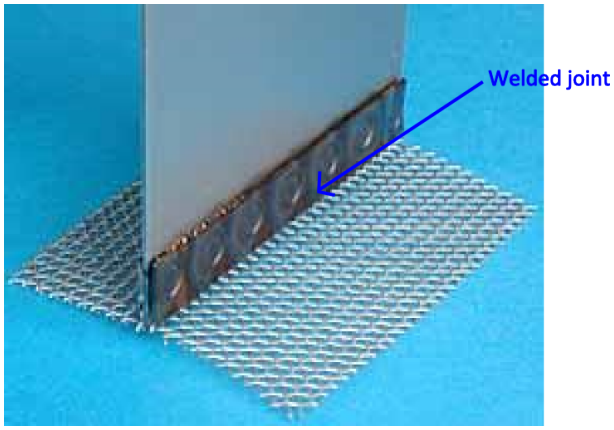

Figure 2.4: Welded joint [17]

2.3 Interference fit

An interference fit is one of the undemountable joints. It uses friction and clamping force to hold the parts together. The clamping force ensues during bonding of both parts together, where a certain part is pushed into a hole of smaller size than the assembly part. Clamping force occurs after cooling and fixes both bonded parts together. Interference fit doesn't allow any relative movements.

2.4 Pins and rivets

Pins are used to connect or attach two parts without any free space between them. It is easy to decompose this type of joint. Shear stress and bearing stress has to be monitored on jointed parts. Rivet should be made of the same material as both jointed parts. These fastenings are loaded by shear stresses. An example of rivet usage is illustrated in Figure 2.5

2.5 Glued joints

Glued joints are undemountable. They equally distribute the loading which is useful in some applications. No stress concentrators occur. Steel and composite are

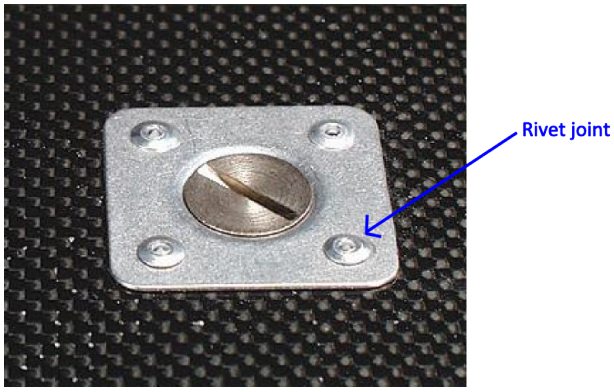

Figure 2.5: Rivets [3]

jointed with glue, by laying composite layups on steel body and hardening or by combination of both methods. It is important, that both surfaces are cleaned well.

A special type of bonding composite to steel was developed by the TWI Company. It is called COMELD and works in similar way as a wall plug. This type of joint is undemountable [15]. The COMELD joint is shown in Figure 2.6.

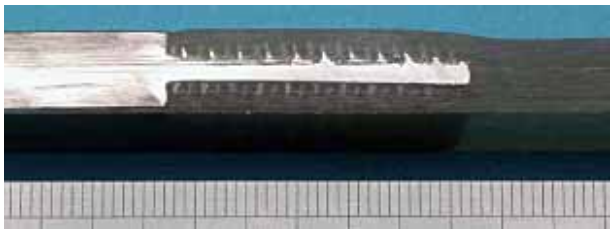

Figure 2.6: COMELD joint [15]

Chapter 3

Carbon fiber reinforced carbon

Fibre composites are materials made from different components with a goal to construct a new material with properties that are better than properties of individual components. Composites are used when the properties of common materials don't satisfy the requirements. Fibre-composites are anisotropic materials, i.e., they have different properties in different directions. Every fibre-composite material consists of two phases, fibres and matrix. During the loading, fibres are the critical phase of a composite. They bear loads in the direction of their orientation. Matrix holds fibres together and is also an important part during transverse loading or during loading in other direction than the fibre direction. One of the most important benefits of fibre composites is their high stiffness and strength at low density. This characteristic is caused by the construction of each composite, which is given by the fibre type, fibre volume ratio, fibre orientation, layer construction, matrix properties and fabricating process. Composites are made by overlaying of fibre layers. It is important how the layers are orientated, because the orientation of the fibres strongly affects composite-behaviour during loading. Even though a lot of different composite types have been developed, only C/C will be discussed more broadly, because it is together with carbon-fibre-reinforced-polymers (CFRP) a material designed for high temperatures and high performance applications. C/C is a composite material which composes of carbon fibres and carbon matrix.

History

The first known product made from carbon fibre (carbonized fibres of cotton and bamboo) was incandescent lamp filament at the end of 19th century [4]. In the following years, composites were used especially in the military industry. Contemporary fibres did not have the same quality as they have today, because they were heated on lower temperatures (only up to 1000 °C). Nowadays, most carbon-fibres are made by carbonizing of polyacrylonitile fibres (PAN) [4]. Rayon or bamboo fibres are used very seldom, because of their nonperfect properties.

Fabrication

Carbon fibre-reinforced carbon material is produced in several steps. Common carbon fibre composite body is fabricated in the first step. Composite body is designed by winding, laminating, pressing or by other method. A material prepared in this way is hardened and pyrolysed[1] and only carbon molecules remain and most of the matrix material disappears.

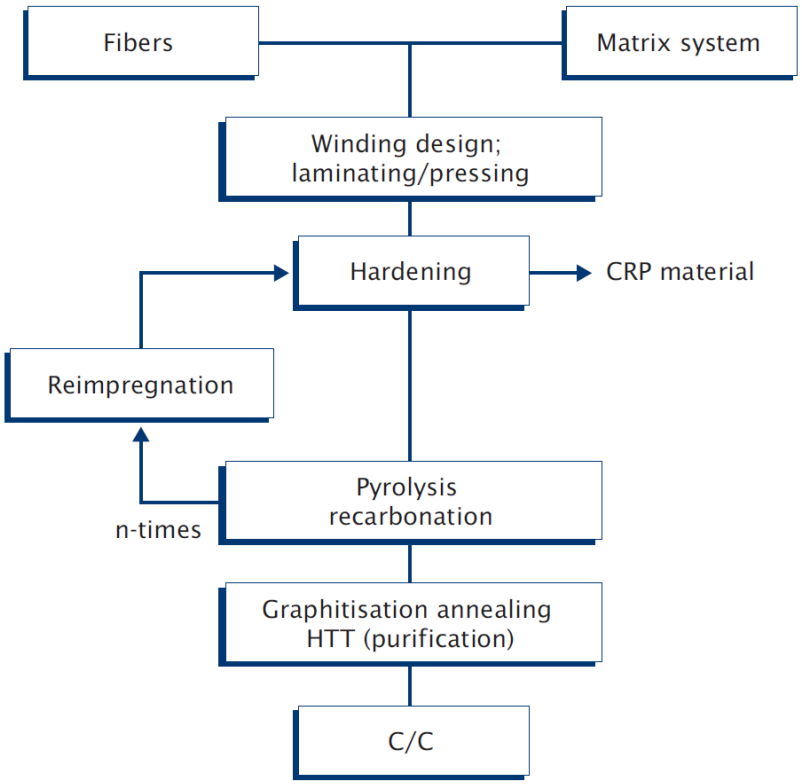

Figure 3.1: C/C fabrication process [9]

All other substances are pyrolysed. Due to pyrolysis, free spaces appear in the material. To fill free places the pyrolysed part is sunk into resin bath and pyrolysed again. This procedure is repeated until the porosity decreases under the required value. Fabrication process is illustrated in Figure 3.1.

Due to pyrolised part corrosion sensitivity, it is common to further modify parts which will appear on air or in other unfavourable conditions. C/C part properties can be improved by for example silicating[2].

[1]Pyrolysis is an endothermic process proceeding in noble gas such as Helium or Argon which decomposites organic materials (on the way to not incinerate [9]) [6].

[2]Silicating is a process, during which, fluid silicon infiltrates into body structure [5].

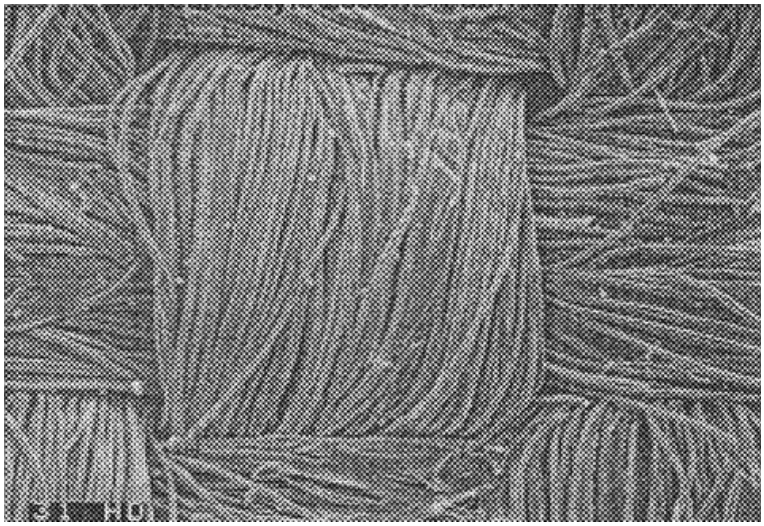

Figure 3.2: C/C under microscope [8]

Properties

C/C is a low density (approximately 2,00 g/cm^3) brittle material with low thermal expansion coefficient [7]. The material is highly resistant to thermal shock and shows high thermal conductivity. C/C reacts with oxygen and is usable at temperatures up to 2800 °C. One of the most important advantages of C/C composites is the possibility to design various shapes. Figure 3.2 shows C/C under microscope.

Application

Nowadays, C/C is not a common material because of its high coasts. It is expensive due to high fibre purchase price and high production costs. C/C composites were originally developed for the aerospace industry. Nowadays, they are also used in other branches, such as automotive industry and aircraft industry (figures 3.3 and 3.4). These branches require light materials resistant to high temperatures.

Figure 3.3: Fixing elements [9]

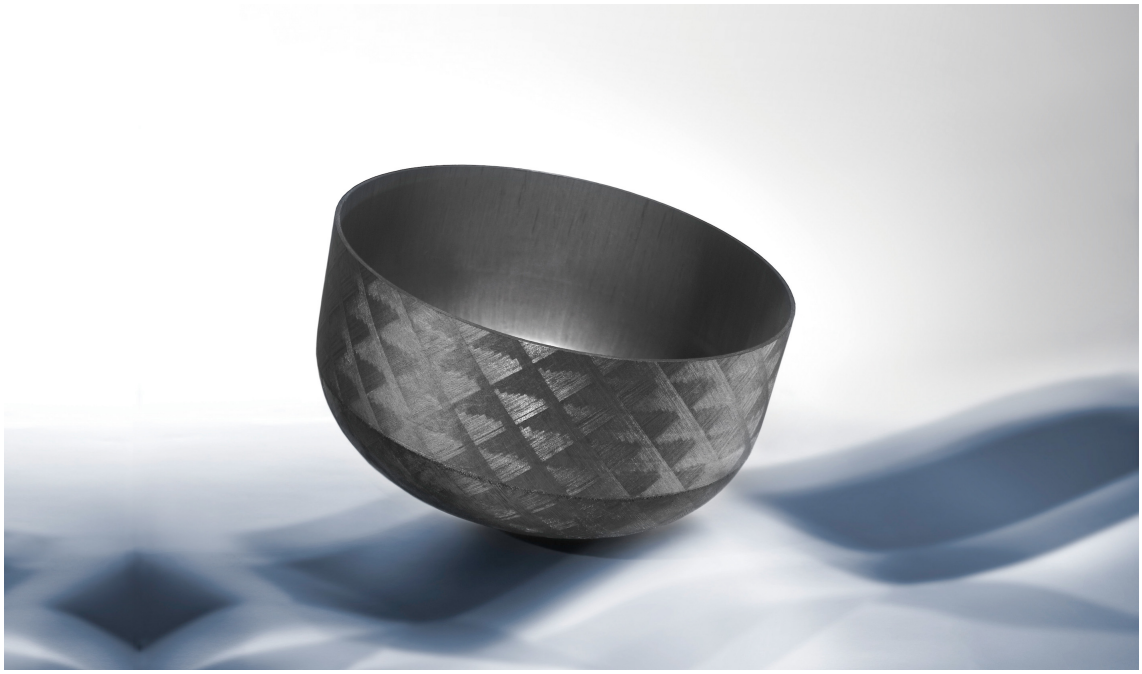

Figure 3.4: A silicating vessel [9]

Chapter 4

Numerical model definition

The task is to model a joint, which is used to link the shaft and the C/C fan for use in high temperature environment. Through this joint, the C/C fan is linked to engine. Problem is solved by using finite element method (FEM) in Abaqus software.

FEM is a numerical method applied in structural mechanics to determine displacements, stresses, loads and other quantities in certain assembly parts. FEM is based on a principle of continuous physical problem discretization into an element mesh. Displacements over elements are approximated by polynomials and stiffness of each element is evaluated. The fundamental static linear problem can be described by the following system of equations

$$\mathbf{K} \cdot \mathbf{u} = \mathbf{F}, \tag{4.1}$$

where $\mathbf{K}$ is a stiffness matrix, $\mathbf{u}$ is a displacements vector and $\mathbf{F}$ is a load vector. Problems with thermal expansion are solved by extension of load vector $\mathbf{F}$ to $\mathbf{F} = \mathbf{f} + \mathbf{t}$, where $\mathbf{f}$ is a real-loads vector and a $\mathbf{t}$ is vector of fictitious forces generated by thermal expansion [13].

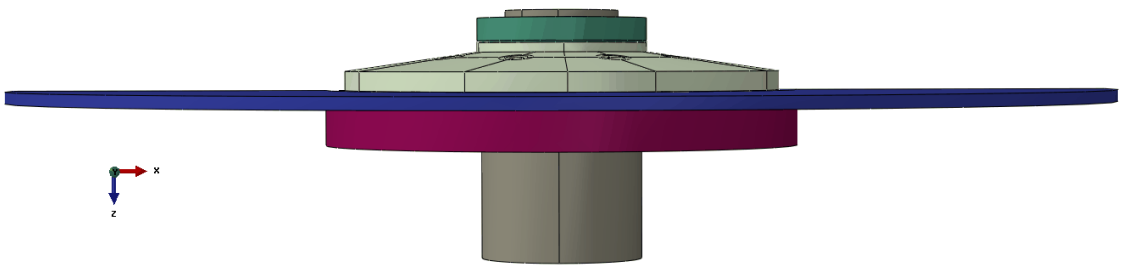

Figure 4.1: Joint assembly

The first step in simulating the fan system in the Abaqus software is the definition of object geometry. The second step is assigning material properties, orientations and

other properties to each part. After that, all parts are assembled and meshed. Then the sequence of loading, boundary conditions and interactions are defined. Finally, the solver is specified.

The original joint assembly composes of 11 parts. The joint assembly is shown in Figure 4.1. The whole system is powered by a shaft, which is joined by bolt joint to the fan. For the stress distribution, flanges were designed. To provide the possibility of rotation and the system stability, key and pins are used.

It was decided to prepare 3 different models. First and second model are very similar and are for this reason described in one section. These two models are used to calculate the pretension force. The third model was created to simulate interaction of pin and composite fan. It is described separately at the end of this chapter.

4.1 Model of joint pretension

First objective of this thesis is to examine which loading or stress occurs in the joint preloaded by stress of 50 MPa. Loading should be examined in a joint, which composes of parts illustrated in Figure 4.1 and in a joint without spring between the flange and the fan. To examine these computations, the two mentioned models were prepared.

The model without spring was used to determine the temperature at which the preload in the joint is zero. The model consists of 5 parts - a shaft, two flanges, a fan plate and a nut.

Model with spring consists of 6 parts - a shaft, a fan plate, a nut, two flanges and a spring. This model is compared with the simpler one and it is also used to demonstrate current situation.

4.1.1 Geometry and mesh

The Key and pins as well as the roundings were suppressed in non-rotating analysis to simplify the model. Mentioned geometry simplifications don't influence the results significantly. Due to geometry symmetry, one half was modelled to reduce computational time. Key and pins are suppressed in both models, because these parts don't transmit any forces during preloading.

The assembly was modelled according to supplied drawings. Parts which weren't included in the drawings and are included in the model were supplemented accordingly with the delivered CAE model.

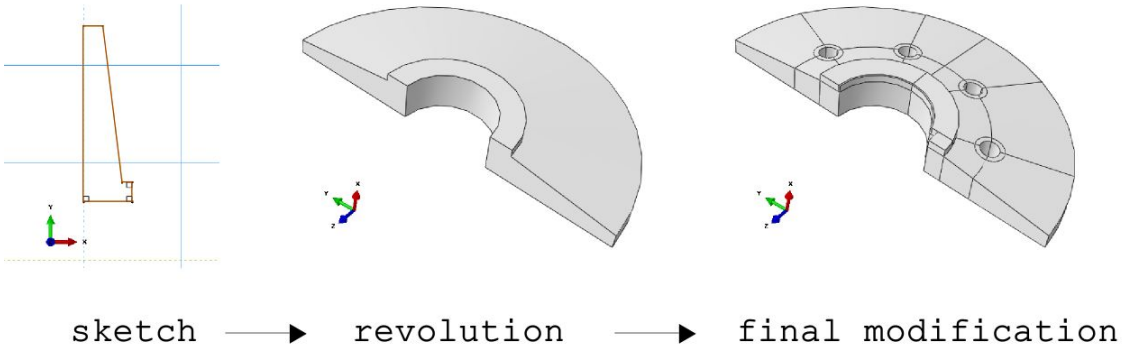

Figure 4.2: Modelling

All parts were modelled as solids by using tool revolution. Section cut was sketched and subsequently rotated along the vertical axes. Parts prepared in this way were than modified to correspond with the real shape and divided into sections for the purpose of better meshing. This process is illustrated in Figure 4.2. After that, parts were meshed using 8-node bricks elements, which means that the model was partitioned into small, more or less regular hexahedrons. Because an inappropriate mesh can create convergence problems and can also influence the results, parts were modified. An example of mesh improvement is shown in Figure 4.3. Element size influences the results as well. It is important to provide the same or at least similar element size in connected boundary areas. Optimally, every border node should find a pair node on the opposite boundary part. Element size of 5 mm was chosen for most of the parts except of the spring, which was meshed by smaller elements due to its size. Finally, the assembly was split into more than 11 000 elements. Generated mesh is shown in Figure 5.2.

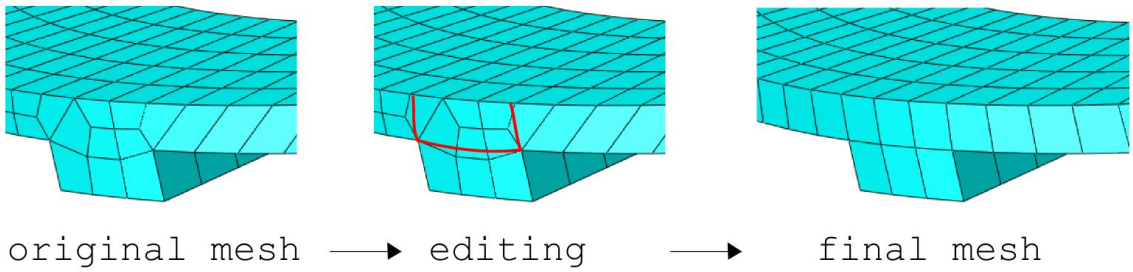

Figure 4.3: Mesh editing

4.1.2 Materials

The whole assembly consists of parts made from two different materials, isotropic steel and 3D-orthothropic C/C composite material.

To describe an mechanical behavior of material, the matrix-form of Hooke's law

$$\sigma = \mathbf{C} \cdot \epsilon, \tag{4.2}$$

can be used [12], where $\mathbf{C}$ is a stiffness matrix. This system of equations can be expressed in inverse form

$$\epsilon = \mathbf{S} \cdot \sigma, \tag{4.3}$$

where $\mathbf{S}$ is a compliance matrix.

Mechanical properties of an isotropic material are the same in all directions and just 2 constants are needed to define this type of material - Young's modulus, E, and Poisson's ratio, ν. Mechanical propertise of orthrotropic material differ in axial directions. Nine constants are necessary to describe behaviour of orthotropic material.

Compliance matrix for an isotropic material is defined as

$$\mathbf{S} = \mathbf{C^{-1}} = \begin{pmatrix} \frac{1}{E} & \frac{-\nu}{E} & \frac{-\nu}{E} & 0 & 0 & 0 \\ \frac{-\nu}{E} & \frac{1}{E} & \frac{-\nu}{E} & 0 & 0 & 0 \\ \frac{-\nu}{E} & \frac{-\nu}{E} & \frac{1}{E} & 0 & 0 & 0 \\ 0 & 0 & 0 & \frac{2+2\nu}{E} & 0 & 0 \\ 0 & 0 & 0 & 0 & \frac{2+2\nu}{E} & 0 \\ 0 & 0 & 0 & 0 & 0 & \frac{2+2\nu}{E} \end{pmatrix}, \tag{4.4}$$

and for an orthotropic material as

$$\mathbf{S} = \mathbf{C^{-1}} = \begin{pmatrix} \frac{1}{E_1} & \frac{-\nu_{21}}{E_2} & \frac{-\nu_{31}}{E_3} & 0 & 0 & 0 \\ \frac{-\nu_{12}}{E_1} & \frac{1}{E_2} & \frac{-\nu_{32}}{E_3} & 0 & 0 & 0 \\ \frac{-\nu_{13}}{E_1} & \frac{-\nu_{23}}{E_2} & \frac{1}{E_3} & 0 & 0 & 0 \\ 0 & 0 & 0 & \frac{1}{G_{23}} & 0 & 0 \\ 0 & 0 & 0 & 0 & \frac{1}{G_{13}} & 0 \\ 0 & 0 & 0 & 0 & 0 & \frac{1}{G_{12}} \end{pmatrix}, \tag{4.5}$$

where E_1, E_2 and E_3 are Young's modules along anisotropy-axis directions, G_{12}, G_{13} and G_{23} are shear modules in isotropy-planes, ν_{12}, ν_{13} and ν_{23} are Poisson's ratios.

In case of a thermal dilatation problem, the deformation vector $\boldsymbol{\epsilon}$ is defined as

$$\boldsymbol{\epsilon} = \boldsymbol{\epsilon_m} + \boldsymbol{\epsilon_t}, \tag{4.6}$$

where $\boldsymbol{\epsilon_m}$ is the vector of deformations caused by mechanical forces and $\boldsymbol{\epsilon_t}$ is the vector of deformations caused by temperature expansion. $\boldsymbol{\epsilon_t}$ is defined using thermal expansion coefficients $\boldsymbol{\alpha}$

$$\boldsymbol{\epsilon_t} = \boldsymbol{\alpha} \Delta T, \tag{4.7}$$

where ΔT is the temperature change.

Thermal behaviour of an orthotropic material is described by thermal-expansion coefficients vector

$$\boldsymbol{\alpha} = \begin{pmatrix} \alpha_1 \\ \alpha_2 \\ \alpha_3 \\ 0 \\ 0 \\ 0 \end{pmatrix}. \tag{4.8}$$

For isotropic materials, $\alpha_1 = \alpha_2 = \alpha_3 = \alpha$.

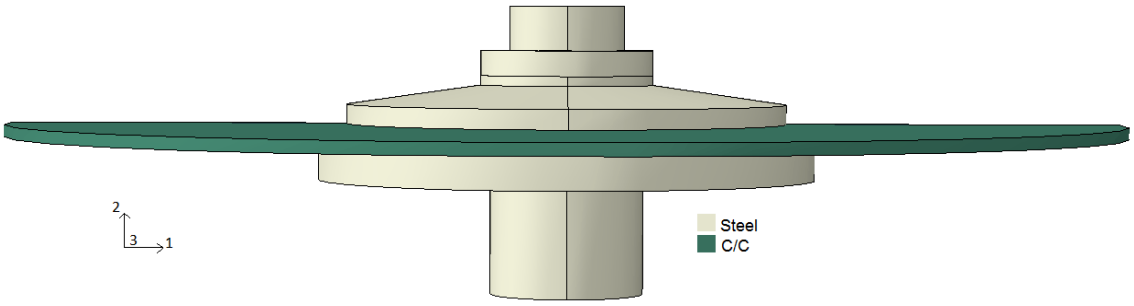

Figure 4.4: Materials in the fan system

Figure 4.4 shows the material distribution in the joint. There, green color represents parts made from C/C composite material CF 226 and grey color stands for parts made from stainless steel X15CrNiSi20-12.

Composite material CF 226 (see Table 4.1) was defined as temperature independent 3D-orthotropic material with a density of $1,55 \cdot 10^{-9}$ kg/m^3. Each composite ply is 0.4 mm thick and is built from woven fabric. Unidirectional fibre composite ply with thickness of 0.4 mm is used in the model. The fan was stacked by 15 of these plies oriented in 0 ° and 90 ° and the spring by 10 of these plies ($[0/90]_{10}$). Anisotropy directions are shown in Figure 4.4.

Stainless steel was defined as an elastic isotropic material. It's mechanical properties as function of temperature were copied from software Deform and the relations are shown in Figure 4.5. The relations of mechanical properties are known just up to 815 °C. Relations for higher temperatures were specified by extrapolation. Material density of used steel is 7600 kg/m^3, Yield strength 205 MPa and Poisson's ratio 0.3.

4.1.3 Step-dependant settings

The fan is assembled and screwed before heating in oven. Numerical analysis was realized to follow this process. The whole simulation was divided into three steps. All these steps diverse in occurring loads, boundary conditions and contacts.

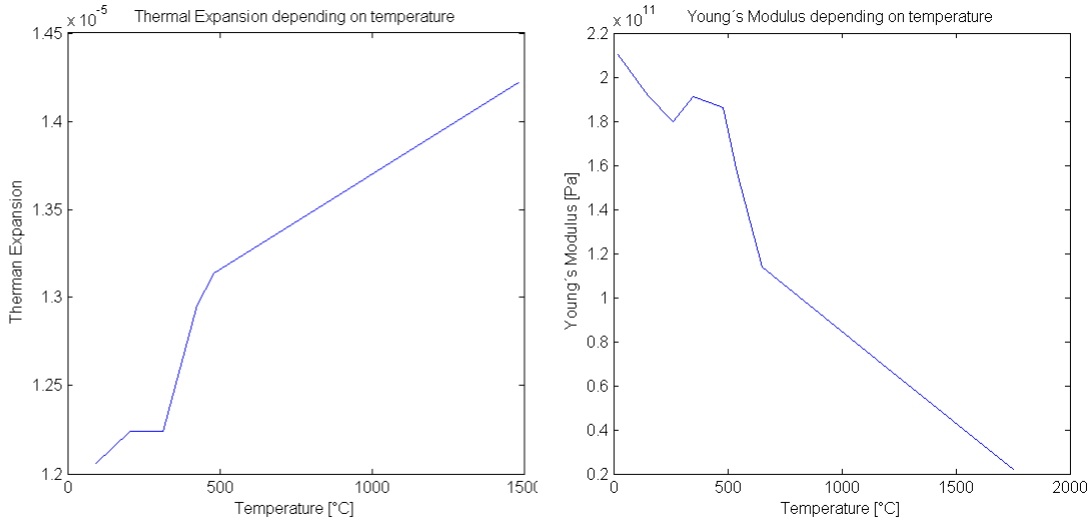

Figure 4.5: Young's Modulus and Thermal Expansion of used steel

E_{1t}=80 GPa	α_1=0.8 $\cdot 10^{-6}$K^{-1}	X_t=110 MPa
E_{2t}=80 GPa	α_2=0.8 $\cdot 10^{-6}$K^{-1}	Y_t=110 MPa
E_{3t}=5 GPa	α_3=7 $\cdot 10^{-6}$K^{-1}	Z_t=3 MPa
G_{12}=5 GPa	ν_{12}=0.07	X_c=100 MPa
G_{13}=2.5 GPa	ν_{13}=0.28	Y_c=100 MPa
G_{23}=2.5 GPa	ν_{23}=0.28	Z_{3c}=160 MPa
S_{12}=18 MPa	S_{13}= S_{23}=8 MPa	

Table 4.1: C/C properties

Step I

This step was used to ensure contact pairs establishment between linked parts. All parts of the assembly were fixed on at least one point. The assembly was symbolically preloaded by pretension of 1 N. In the real assembling, there is no equivalent step. This step was realized just for convergence of the numerical simulation.

Pretension was implemented using Bolt load tool. Preloaded shaft part was partitioned into two pieces. Half of the distance between the bolt head and the end of the screw determined the surface of partitioning. Two obtained adjacent surfaces were moved by the bolt load against each other until desired pretension was reached (see Figure 4.7).

Surface to surface contact was defined between all neighbouring surfaces except of the nut-shaft connection. The friction coefficient was defined as 0.1, which is a common value for two steel parts. Further, the interaction doesn't allow any

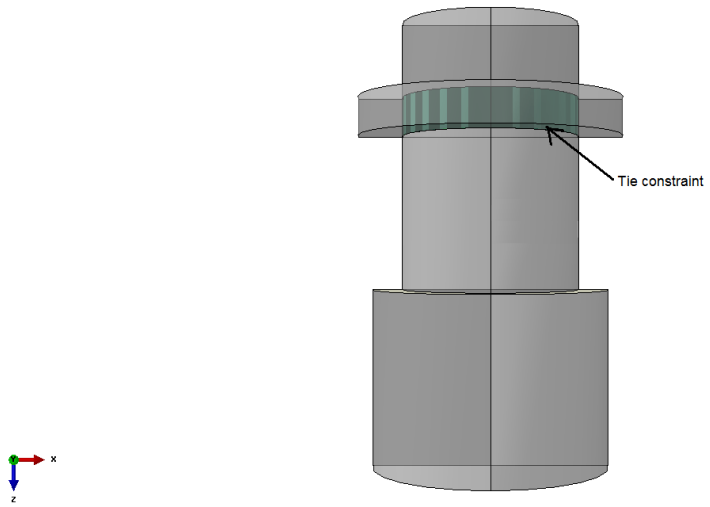

Figure 4.6: Tie surfaces

penetrations between linked parts. The tie constraint is between the shaft and the nut and simulates a fixed connection. This constraint doesn't allow any relative movements. Tie surfaces are shown in Figure 4.6.

The whole under surface of the shaft was fixed in vertical direction and the middle point of this surface was fixed in all directions. To assure numerical analysis convergence, all parts were fixed in at least one point. Boundary conditions following the symmetry in cut-plane were also defined in this step.

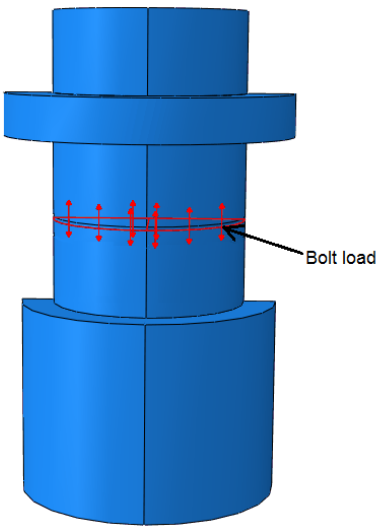

Figure 4.7: The bolt load surface

Step II

In this step, stress of 50 MPa generated by bolt load was reached. Because a bolt load is specified by the load, compressive stress was converted into a force F using the following equation

$$F = \sigma \cdot S, \tag{4.9}$$

where σ is the defined stress ($\sigma = 50$ MPa), and S is the surface area, where pretension occurs ($S = 2827$ mm^2). Force magnitude of approximately 70 kN was obtained. As a result of the mentioned load, a new interaction between the lower flange and the fan occurs. One point fixation of all parts except of the shaft is deactivated in this step.

Step III

In this step, temperature in each node of the assembly was raised up to 1500°C. Relative displacements of adjacent surfaces on the shaft causing pretension were fixed. All boundary conditions and interactions remain the same as in the previous step.

4.2 Interaction between C/C plate and pin

The next goal of this thesis is to simulate the interaction between the C/C part and pins during rotation. Assembly consisting of two parts - the C/C plate and the pin was created. The C/C plate is a cut out from the C/C plate used in previous two models. It also composes of 15 plies oriented in directions 0° and 90°. The pin was modelled as an undeformable rigid body. The assembly is shown in Figure 4.8. A step defined by loads at ends of the pin was created. The force applied to the pin was computed from the engine load. The torque of the engine is 36 Nm by 2940 revs. The fan rotates with angular velocity of 2300 revs. The Torque M was obtained according to the following equation

$$M = \frac{36 \cdot 2940}{2300} \doteq 46 \text{ Nm}. \tag{4.10}$$

The torque is divided between 8 pins, which are located in distance of 6,5 cm from the rotation-axis. Pin load was defined as

$$F_{1p} = \frac{F_1 \cdot SF}{2 \cdot n} = \frac{707,7 \cdot 1,5}{2 \cdot 8} \doteq 66,3 \text{ N}, \tag{4.11}$$

where SF is safety factor 1.5, n is the number of pins, and F_1 is defined as

$$F_1 = \frac{M}{u} = \frac{46}{0.065} \doteq 707,7 \text{ N}, \tag{4.12}$$

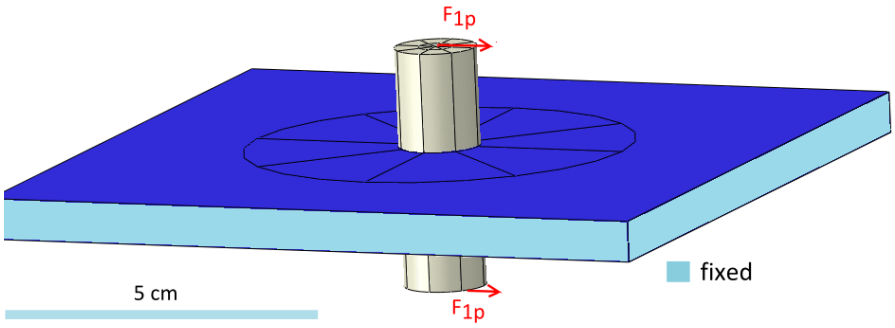

Figure 4.8: Interaction between the C/C plate and a pin

where u is the pin distance from the rotation axis.

To consider different orientation of the load transferred from the loaded pin to the plate with respect to the fibre orientation of the plate, two tasks were created. Firstly force was applied in the same direction as the fibre orientation and secondly under angles of $\pm 45°$ with respect to the fibre direction. Loading caused by pretension wasn't considered in this model.

Chapter 5

Results

This chapter summarizes results from all three models. To quantify stress in all parts, failure criterions Tsai-Wu and Von Mises were used.
Von Mises failure criterion is an energy criterion. It estimates that, material is safe until the yield distortion energy specified for the used material is higher than the maximal value of real distortion energy.
The equation for Von Mises criterion is

$$\sqrt{\sigma_1^2 + \sigma_2^2 + \sigma_3^2 - (\sigma_1\sigma_2 + \sigma_2\sigma_3 + \sigma_3\sigma_1)} \leq \sigma_y, \tag{5.1}$$

where σ_y is yield strength, which is $\sigma_y = 205$ MPa for the used steel and σ_1, σ_2 and σ_3 are principal stress values. This criterion was used for parts made of steel.
Tsai-Wu is a failure theory designed for anisotropic materials. The criterion is specified by following equation [16]

$$f_i\sigma_i + f_{ij}\sigma_i\sigma_j = 1;\ i, j = 1, 2, 3, 4, 5, 6 \tag{5.2}$$

where coefficients f_i and f_{ij} are determined experimentally. If some coefficients are not known, they can be computed using following formulas:

$$f_1 = \frac{1}{X_t} - \frac{1}{X_c},\ f_2 = \frac{1}{Y_t} - \frac{1}{Y_c},\ f_3 = \frac{1}{Z_t} - \frac{1}{Z_c},\ f_4 = f_5 = f_6 = 0, \tag{5.3}$$

$$f_{11} = \frac{1}{X_t \cdot X_c},\ f_{22} = \frac{1}{Y_t \cdot Y_c},\ f_{33} = \frac{1}{Z_t \cdot Z_c}, \tag{5.4}$$

$$f_{44} = \frac{1}{S_{23}^2},\ f_{55} = \frac{1}{S_{31}^2},\ f_{66} = \frac{1}{Su_{12}^2}, \tag{5.5}$$

$$f_{12} \backsimeq -\frac{1}{2\sqrt{f_{11}f_{22}}},\ f_{13} \backsimeq -\frac{1}{2\sqrt{f_{11}f_{33}}},\ f_{23} \backsimeq -\frac{1}{2\sqrt{f_{22}f_{33}}}, \tag{5.6}$$

where X_t, Y_t and Z_t are tensile strengths in corresponding directions, X_c, Y_c and Z_c are compression strengths in corresponding directions, τ_{12} is shear strength in plane direction and S_{13} and S_{23} are inter-laminar shear strengths.

Critical value is for Tsai-Wu criterion number 1.

5.1 Joint pretension simulation

To qualify both models, relation between bolt pretension and temperature as well as Tsai-Wu and Von Mises criterion values were examinated.

Displacements

Displacements magnitudes after the second step (pretension) are displayed in Figures 5.1 and 5.2. The most considerable displacement affects on parts substructures, which are pressed down by the tool bolt load. The displacement values are higher in the model with a spring, because stiffness of the spring is lower than stiffness of other parts of the assembly.

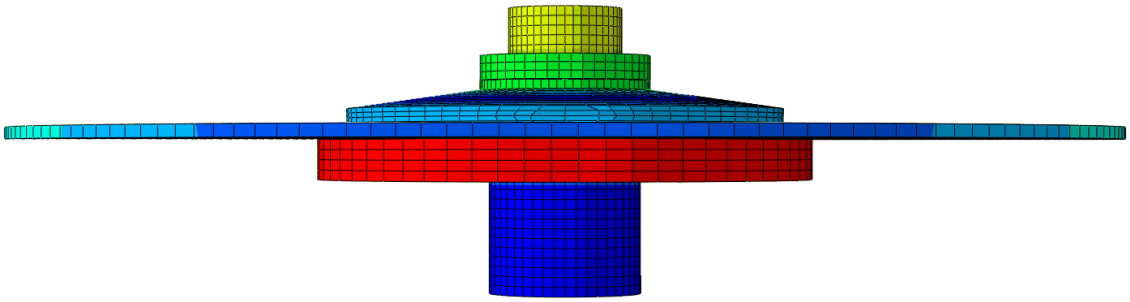

Figure 5.1: Displacements after the second step in the model without a spring

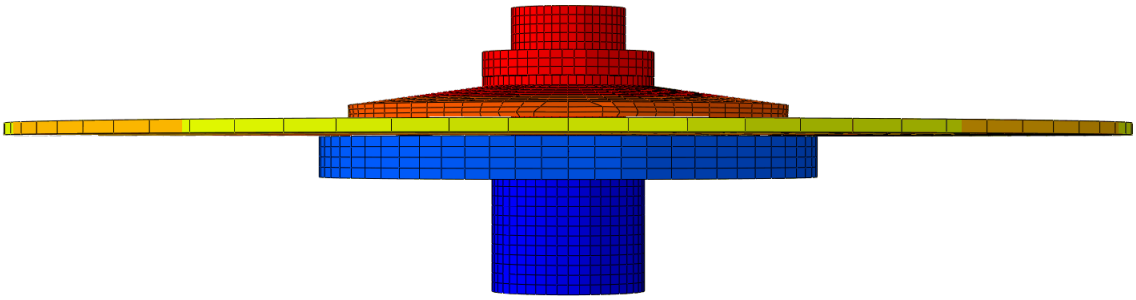

Figure 5.2: Displacements after the second step in the model with a spring

In Figures 5.3 and 5.4 displacements on the end of the third step are shown. The figure for model without spring represents temperature of 1004 °C, which is the highest temperature when preload occurs. The graphic of the model with a spring represents temperature of 1500 °C. Displacements in both models are higher in the third step than in the previous one. These displacements are caused by thermal expansion. Relative displacements between the fan plate and the middle surface of the shaft are close to zero in temperature of 1004 °C in the model without a spring.

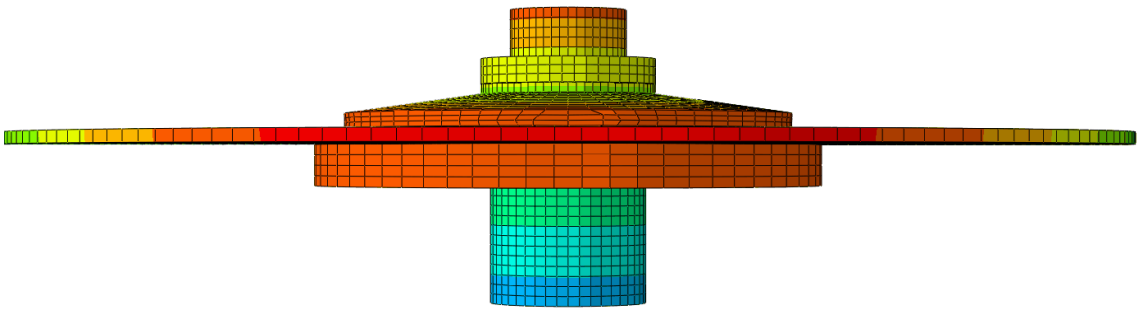

Figure 5.3: Displacements at 1004°C in model without spring

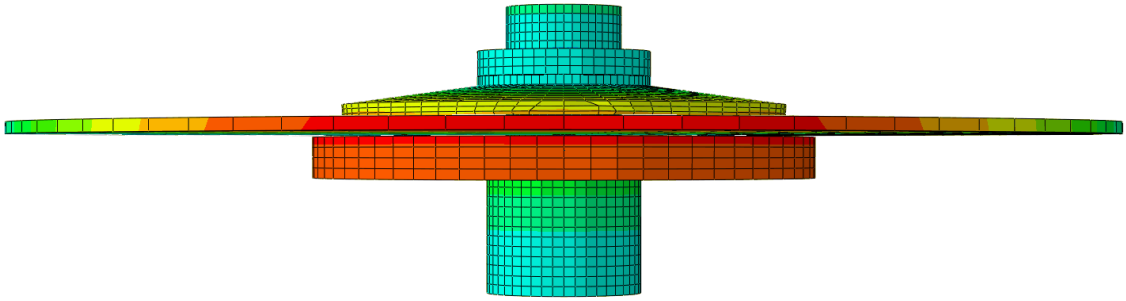

Figure 5.4: Displacements at the temperature of 1500°C in the model with a spring

Stress

Stress was reviewed in metal parts and C/C parts separately. Von Mises failure criterion was used to quantify stress in metal parts. Figures 5.5 and 5.6 show stress in both models after the second step (pretension). The highest value of Von Mises failure criterion is 183 MPa, whereas critical value for used steel is 205 MPa. This implies that occurring stress values are not critical. Note that the maximum service temperature of used steel is 1100 °C and the melting point is 1450 °C. That is why values for temperatures close to the temperature of 1500 °C should be taken tentatively.

Tsai-Wu failure criterion values are shown in Figure 5.7. This figure shows the maximal absolute Tsai-Wu value over all plies (envelope) after pretension in the model without a spring. Largest stresses occur in the middle area of the plate. Because local failures are allowed in the middle area of the fan plate, Tsai-Wu values in these areas were not evaluated. According to Figure 5.7, the highest Tsai-Wu criterion value on the C/C plate is approximately 0.34, which is a safe value. However, the magnitude of the highest value occuring on the C/C plate in the model with a spring is 5.6. This implies, local failures arise on the plate. Those failures are caused by the spring.

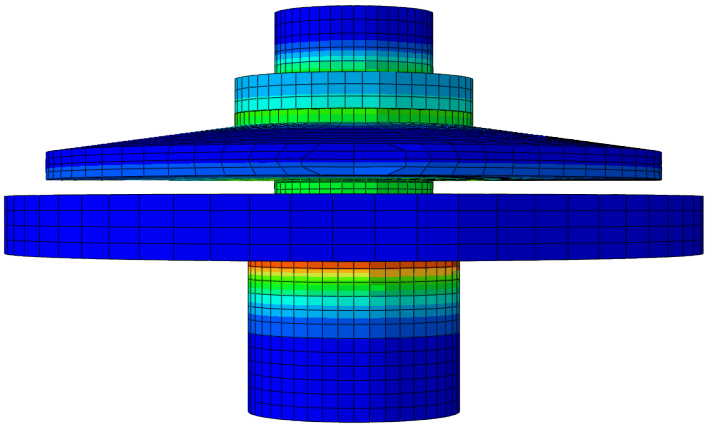

Figure 5.5: Von Mises stress after pretension in model without spring

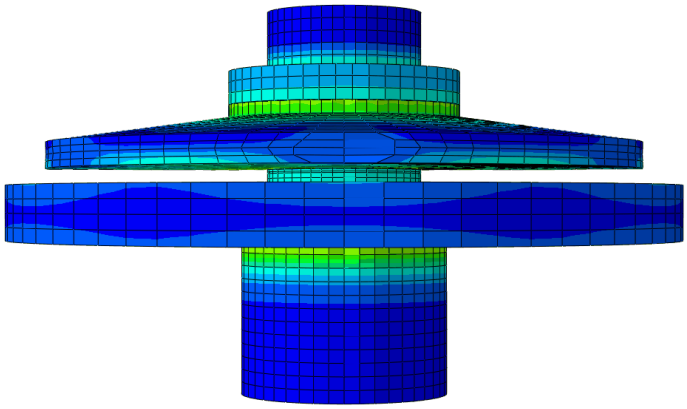

Figure 5.6: Von Mises stress after pretension in model with spring

The highest Tsai-Wu envelope value in the spring part reaches number of 223, which is much over the highest permissible Tsai-Wu value equal 1. Tsai-Wu criterion is evaluated after the numerical simulation and doesn't consider a material failure and stress redistribution during the simulation. Simulation with progressive failure should be performed for more precise results, but this exceeds scope of this work.

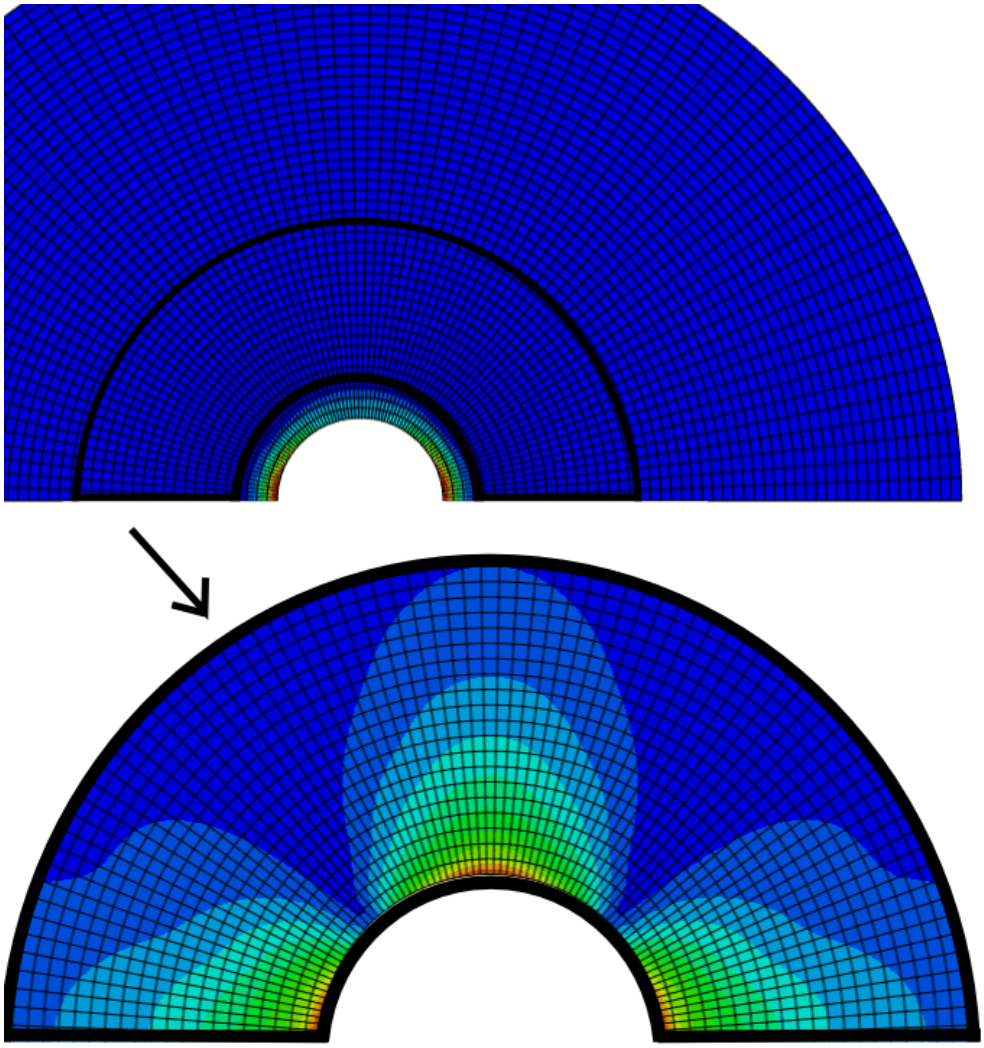

Figure 5.7: Tsai-Wu values in the model without spring

Spring part shape adjustment

Because the Tsai-Wu limit value in the spring part was exceeded hundredfold, models with adjusted spring shapes were modelled and compared in order to find a construction with better behaviour properties. The overview of spring shape parameters, resulting Tsai-Wu envelope values and pretension force are in Table 5.1. Lowest Tsai-Wu value equal 9.8 occurring on the spring part was reached in the model with a ring with the same dimension as the original spring's. Dependency of pretension force on temperature for model with a C/C ring is shown in Figure 5.8.

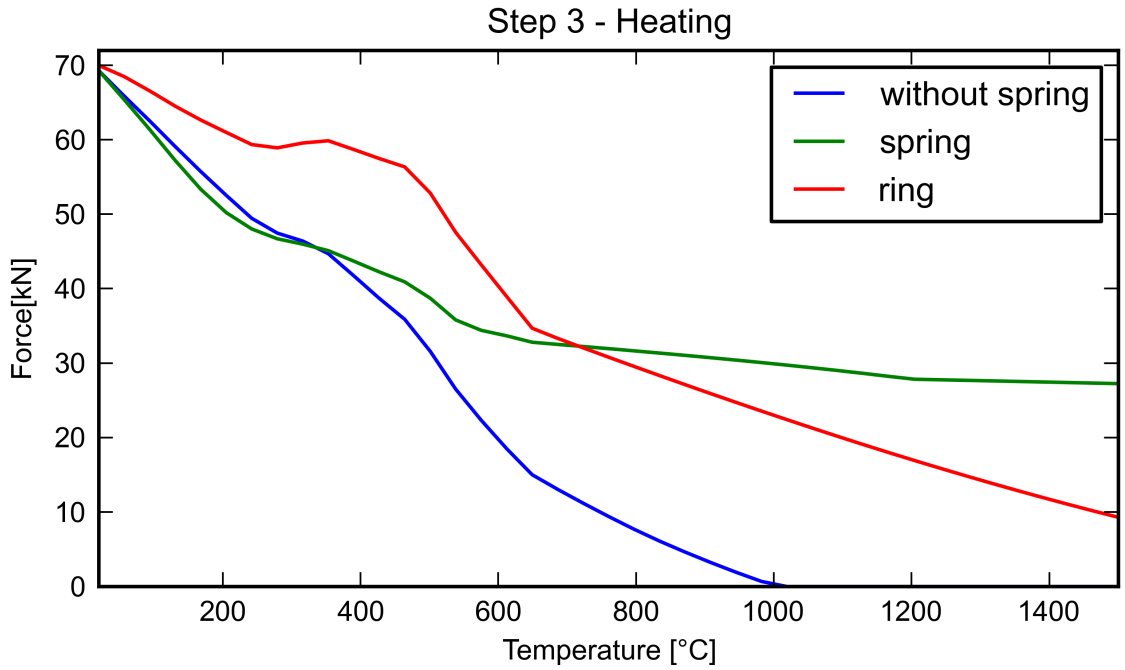

Figure 5.8: Relationship between pretension and temperature

Bolt pretension

A very important parameter of a bolt joint is the pretension force. This force changes due to different thermal expansion coefficients of used materials. Because thermal expansion coefficient value of metal parts is higher that of C/C parts, the magnitude of occurring force with raising temperature decreases. This situation is shown in Figure 5.8. The blue curve represents the relation between pretension force and temperature in the model without a spring. The green curve shows this relation for the model with a spring and the red one relation for the model with a ring. This plot shows that pretension in the model without a spring is higher than in model with a spring up to 333 °C. Pretension value falls to zero in model without spring at temperature of 1004 °C. At higher temperatures than 1004 °C, individual parts can move and are not firmly linked to other parts of the assembly. Because the solution of computation of the problem with free moving parts diverges, 1004 °C is the highest temperature, for which stress and other magnitudes were computed. Even though the pretension in the model with a spring stays relatively high even at high temperatures, it has to be considered that, according to Tsai-Wu, failures occur on the spring, which influences stiffness of the spring and its behaviour. Pretension values in model with ring are lower than in the model with a spring, but these values can be considered relevant, because Tsai-Wu values on the ring are not as high as in the case of the model with a spring.

5.2 Pin and C/C plate

Figures 5.9 and 5.10 show envelope Tsai-Wu criterion values in the C/C plate. First figure shows Tsai-Wu criterion values for all layers in composite with fibres oriented in the direction of the force. Second figure illustrates also Tsai-Wu criterion values, but in composite with layers oriented in angle $\pm 45\,^{\circ}$ relative to force direction.

Results show that the thickness of the C/C plate is in both cases overlarged. The highest value reaches $7 \cdot 10^{-3}$. Note that in the model of the C/C plate and the pin, pressure affecting on the C/C plate through pretension was not considered.

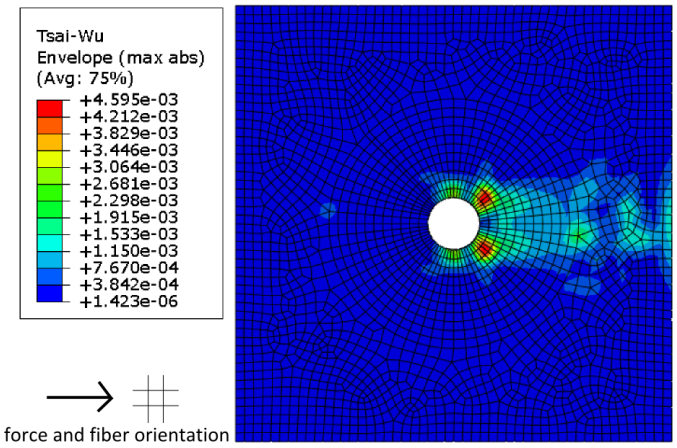

Figure 5.9: Tsai-Wu failure criterion for force oriented in the fibre direction

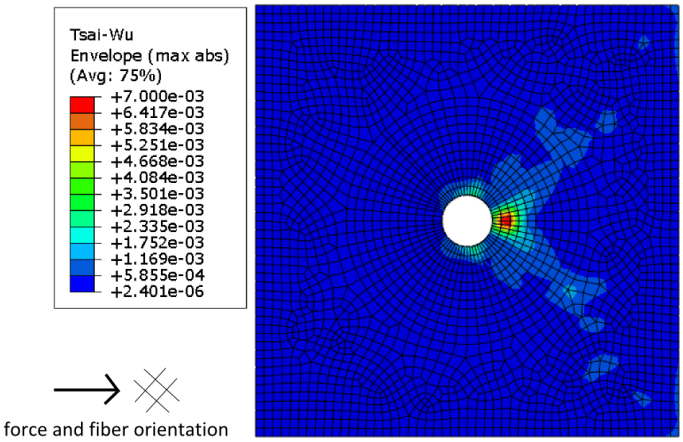

Figure 5.10: Tsai-Wu failure criterion for force oriented in $\pm 45\,^{\circ}$ relative to the fibre direction

Outer spring diameter [cm]	10	10	10	10	11.5	10
Inside spring diameter [cm]	12	12	6	8	9.5	8
Profile depth [cm]	0.4	0.2	0.4	0.4	0	0
Maximal spring part Tsai-Wu envelope value	228	300	244	21	10	10
Maximal fan part Tsai-Wu envelope value	5.9	17	3.5	16	1.3	0.5
Pretension force at the temperature of 1500 °C [kN]	30.705	41.213	11.888	16.120	9.008	9.303

Table 5.1: Values for different types of spring components

Chapter 6

Conclusion

This work is focused on modelling a bolt joint joining a composite fan and a metallic shaft. Three models were proposed, first two represent two different variants of a simplified joint, while the third one represents the interaction of the fan bottom plate and pins connecting flanges and the fan.

Displacements, stresses and dependencies of pretension force on temperature were evaluated for the first two models. Results show that the simpler joint design, without the spring, is sufficient in lower temperatures. The limit temperature for use of the joint without spring can be considered nearing 1000 °C. By this temperature the thermal expansion of steel parts is so high that the contact force between individual parts vanishes and the joint looses it's functionality. Generated stresses by this temperature can be considered as acceptable. This behaviour is in agreement with experience of the Schunk Kohlenstofftechnik GmbH company.

The results for model with spring show higher pretension forces for temperatures above 300 °C. However, interpretation of results for this model is problematic due to high stresses in spring part and its failure. That is why, shape of the spring part was modified and results were reevaluated. Best behaviour was achieved with ring shape spring, but stress criteria values remain critical and change of whole joint design should be considered.

All three models were simplified. Two material behaviour were not considered; plasticity, the inability to return to original size after the load is removed, and creep, permanent deformation caused by loading in high temperatures. Moreover, material properties were assumed and should be replaced by values from measurement. Additionally, progressive failure should be implemented in material model. Considering all these phenomenons would improve the model precision but would in turn make the problem more complicated.

In agreement with the internal policy of the company Schunk Kohlenstofftechnik

GmbH regarding third party access to company's internal information and the decree of the University of West Bohemia, sections containing confidential information were removed from the published version of this thesis.

List of Figures

Bibliography

[1] http://en.wikipedia.org.

[2] http://www.designnews.com.

[3] http://www.pro-werks.com.

[4] Historical Overview of the Carbon Fiber Composites Industry. [online], last seen 5/2014.

[5] Silizieren, Lexikon der Gleitringdichtung. [online], last seen 5/2014.

[6] Dr.-Ing. Gerd-Peter Bracker. Pyrolyse: Eine Technologie fuer das 21. Jahrhundert.

[7] Padmayya Naik et al. A Study On Carbon Fiber Reinforced Carbon Composites For Structural Applications. *International Journal of Engineering Science and Technology (IJEST), 3670*, 5 May 2011.

[8] R. C. Gaffney, J. J.; Loszewski. Carbon-Matrix Composites, Compositions and Methods Related Thereto. *United States Patent No. US 6,638883 B2*, 28 October 2003.

[9] Schunk Kohlenstofftechnik GmbH. Schunk/Carbon fiber-reinforced carbon (C/C). 2011.

[10] K. Kalab. Části a mechanismy strojů pro bakaláře, části spojovací. *Vysoká škola báňská - Technická univerzita Ostrava*, 2007.

[11] R. Kottner. Spojování strojních částí z izotropního a anizotropního materiálu. *Písemná práce ke státní doktorské zkoušce*, 2004/2005.

[12] Vladislav Laš. *Mechanika kompozitních materiálů.* Západočeská univerzita v Plzni, 2004.

[13] G. P. Nikishkov. Introduction to the Finite Element Method. *Lecture Notes, University of Aizu, Japan*, 2007.

[14] Saether E. S. Cheng D. Ramkumar, R. L. Design guide for bolted joints in composite structures. 1986.

[15] F. Smith. COMELD - An innovation in composite to metal joining. *Composites Processing 2004*, April 2004.

[16] S. W. Tsai. *Strength life of composites*. Stanford University.

[17] Staines D. J. W M Thomas, W.M. Transition joints between dissimilar materials, 2006.